Flow rate measurements in isolated perfused kidney tubules by fluorescence photobleaching recovery

Bruno Flamion,* Peter M. Bungay,‡ Carter C. Gibson,* and Kenneth R. Spring*
*Laboratory of Kidney and Electrolyte Metabolism, National Heart, Lung, and Blood Institute, and ‡Biomedical Engineering and Instrumentation Program, National Center for Research Resources, National Institutes of Health, Bethesda, MD 20892

ABSTRACT We have developed a new application of the fluorescence photobleaching recovery (FPR) technique for instantaneous measurement of volume flow rates at any axial position along isolated perfused kidney tubules. The method requires fast data acquisition of emitted fluorescence through a photomultiplier (time resolution, 0.5 ms) coupled with differential interference contrast microscopy to measure luminal diameters accurately. While the tubule is perfused in vitro with an impermeant fluorophore (fluorescein sulfonate), a 20-ms bleach pulse reduces the fluorescence in the observation region by 20–25%. Fluorescence recovery is a direct function of perfusate velocity; diffusion plays no significant role in the early phase of recovery. A fluid dynamics approach to data analysis shows that fractional recovery increases linearly with time until $t = L/2v_m$, where L is the length of the observation window and v_m is the mean axial velocity. Practically, a linear regression analysis of the early recovery phase allows measurement of v_m of up to 0.14 cm/s, i.e., a 40-nl/min flow rate in a 25-μm-diameter tubule. Calibration experiments in small glass tubes perfused at predetermined flow rates demonstrated good accuracy (within 10%) and reproducibility (coefficient of variation, 8.7%). In rat inner medullary collecting ducts microperfused at 4–40 nl/min, the correlation with a standard fluid collection method was excellent ($r^2 > 0.97$). The method should also be suitable for the direct measurement of fluid flow rate in kidney tubules or blood vessels microperfused in vivo.

INTRODUCTION

The technique of in vitro microperfusion of isolated kidney tubules (Burg. et al., 1966) has long been a standard method for the study of single nephron function in a controlled environment. Recent advances in fluorescence microscopy have increased the scope, and also the time resolution, of this technique. In particular, changes in rates of fluid transport across the epithelium can now be discriminated within seconds (Kuwahara et al., 1988), creating the need for faster and more accurate measurements of perfusion flow rates. The time-honored method of collecting the perfused fluid at the distal end of the tubule has a poor time resolution and cannot be easily linked to the observation of fluorescence in a defined portion of the tubule lumen or within individual cells.

Fluorescence photobleaching recovery (FPR), also known as fluorescence recovery after photobleaching (FRAP), is an optical technique developed during the 1970's to measure lateral diffusibility of macromolecules in cell membranes (Peters et al., 1974; Axelrod et al., 1976; Edidin et al., 1976; Jacobson et al., 1976). Since then, its scope has expanded tremendously; different FPR patterns and the addition of digital imaging have made it possible to explore a variety of cellular dynamic processes such as microtubule assembly (Salmon et al., 1984), nucleocytoplasmic flux (Peters, 1984), or gap junction-mediated communication between cells (Wade et al., 1986). More recently, a video digitization modification of FPR was used for measuring in vivo interstitial fluid convection in normal and neoplastic tissues (Chary and Jain, 1989), as well as binding parameters (Kaufman and Jain, 1990). Video image analysis, however, limits the range of measurable convective velocities to ≈0–2 μm/s (Chary and Jain, 1989). The versatility of the FPR technique has prompted us to investigate its use in the determination of volumetric flow rates in microperfused tubules.

In a conventional spot photobleaching experiment, an attenuated laser beam is focused to a diffraction-limited spot in a uniformly fluorescent sample and the emitted fluorescence is monitored as a function of time. Then, a sudden and brief increase in laser power irreversibly bleaches a fraction of the fluorophore within the spot. After bleaching, the time course of fluorescence recovery is followed with the same attenuated laser beam. Recovery results from movement of fluorescent molecules into the bleached area either by diffusion or through a systematic transport process such as convective flow. Detailed analyses of theoretical photobleaching recovery curves have been developed by Axelrod et al. (1976) for a laser beam of either Gaussian or uniform circular disc profile.

We present here a different version of FPR, based on bleaching a dye solution flowing through an isolated perfused tubule. Using a photomultiplier tube, fluorescence recovery is monitored with a 0.5-ms time resolu-

0006-3495/91/11/1229/14 $2.00

tion. The geometry of the specimen and the extremely fast time course require a different optical arrangement and approach to data analysis. Fluorescence recovery was found to be a direct function of fluid velocity in the tubule, as confirmed by in vitro calibrations using perfused glass capillary tubes.

METHODS

Optics and electronics

Fig. 1 is a schematic overview of the optical and electronic system. The beam from a 200-mW argon ion laser (Omnichrome, Chino, CA) is first passed through an acousto-optic modulator, which controls both wavelength selection and output intensity with a 25-μs time resolution (Spring and Smith, 1987). For the experiments described here, only the 488-nm line was used. To provide uniform illumination, as initially suggested by Ellis (1979), the beam is then focused (through *lens L1* in Fig. 1) onto the end of a flexible single-fiber light guide. Vibrating the fiber, by wrapping it around the cooling fan of the laser head, assures phase randomization of the light beam, as attested by the disappearance of the speckle due to the coherence of laser light. The light emerging from the fiber is collected by a collimating lens (*L2*) and directed through a slit diaphragm into the epi-illumination port of an inverted microscpe (Nikon Diaphot, Nikon Microscope Inc., Garden City, NY) mounted on a pneumatic isolation table. The rectangular slit diaphragm, which can be adjusted manually, is used as a field stop to define the illumination window overlapping a portion of the tubule (see Fig. 2). A relay lens (*L3*; infinity corrected) directs the beam to a dichroic mirror, where it is reflected to the specimen through a 100×/1.32 N.A. planapochromat oil-immersion objective (Leitz Inc., Rockleigh, NJ). Provided axial alignment is carefully adjusted, the illumination profile in the focal plane is fairly homogeneous, as revealed by digital imaging analysis (see Fig. 7).

The emitted fluorescence, collected with the same objective, is transferred to the camera port of the microscope and partitioned by a 50/50 beam splitter between a photomultiplier tube (Type 9826B, Thorn EMI Gencom Inc., Fairfield, NJ) and a CCD camera (Model CCD-72, Dage MTI Inc., Michigan City, IN) coupled to an image intensifier (Model KS-1381, VideoScope, Washington, DC). For fast monitoring of fluorescence, the amplified and RC-filtered output of the photomultiplier is digitized and interfaced to an IBM PC/AT through a data acquisition system (Model DAS 570, Keithley Metrabyte, Taunton, MA). Counting interval is set to 0.5 ms. A fast electro-optic shutter (Model LV500A, Displaytech Inc., Boulder, CO; *S1* in Fig. 1) protects the photon detector from the high level of fluorescence emitted during the bleach pulse and from any bright transmitted light (see below). When spatial assessment is needed, the intensified CCD camera is used to capture low light level fluorescence

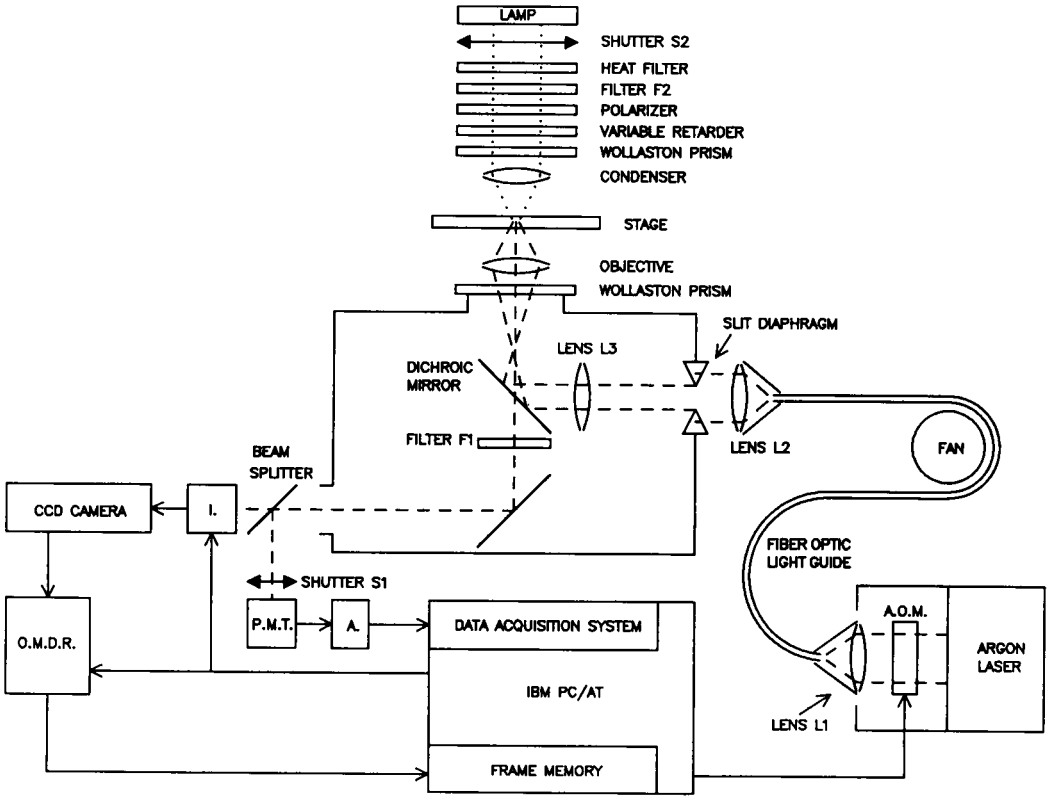

FIGURE 1 Diagram of the experimental setup. Abbreviations are as follows: *A.*, current-to-voltage amplifier; *A.O.M.*, acousto-optic modulator; *I.*, image intensifier; *O.M.D.R.*, optical memory disc recorder; and *P.M.T.*, photomultiplier tube. The different components are described in detail in the text. The *dotted lines* represent the DIC illumination light path; the *dashed lines* are the paths of laser light epi-illumination, emitted fluorescence, and DIC transmitted light.

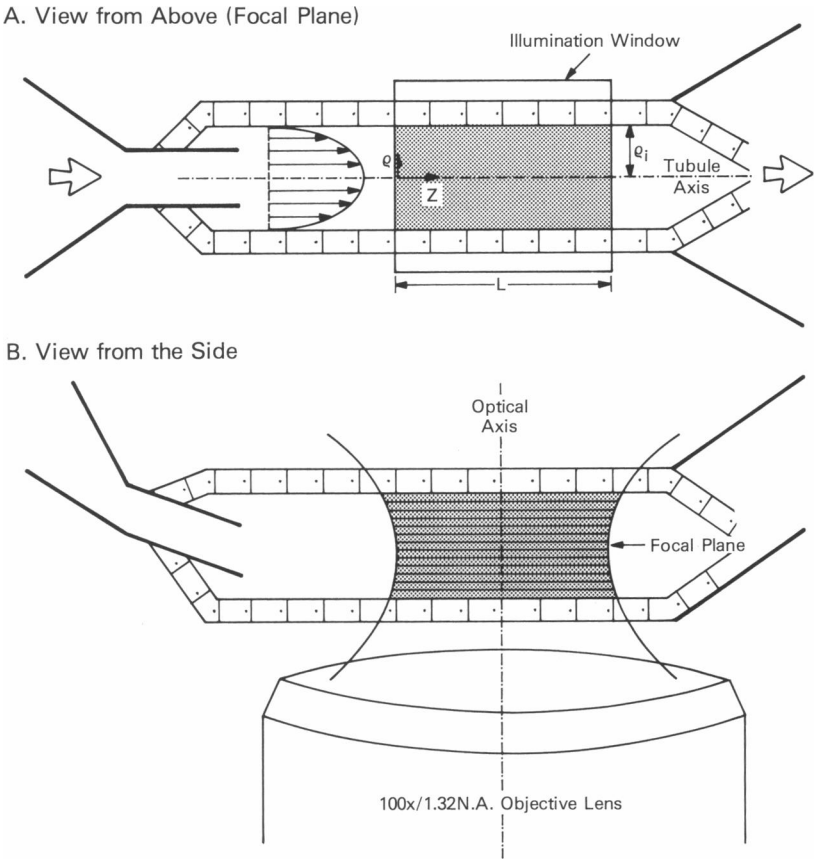

FIGURE 2 Horizontal (*A*; *focal plane*) and vertical (*B*; *optical axis*) cross-sections through an isolated perfused tubule, illustrating the illumination and fluorescence collection geometries. ρ and z are the radial and axial coordinates, respectively; ρ_i is the inner tubule radius; L is the length of the illuminated window as defined by the rectangular image of the field diaphragm in the focal plane. The gray areas represent the volume of illuminated fluorophore. A schematic parabolic velocity profile is shown in *A*. In *B*, the horizontal lines in the illuminated region schematize the stack of optical sections used to assess the spatial distribution of light intensity and photobleaching in a model tubule as detailed in the text.

images, which are stored on an optical memory disc recorder (Model TQ2028F, Panasonic Industrial Co., Secaucus, NJ).

To measure tubule diameters with the highest accuracy, the microscope is also equipped for transmitted light imaging with differential interference contrast (DIC) in a way that allows simultaneous DIC and fluorescence microscopy without major light loss (Spring, 1990). Briefly, the dichroic mirror in the epi-illumination filter cube acts as an analyzer in the polarized transmitted light path for a narrow range of wavelengths included in the spectral separation between the mirror's "*P*" plane and "*S*" plane transmission curves. The original DIC analyzer, which would impede the collection of emitted fluorescence, can thus be removed. The choice of filters is dictated by the fluorophore. In the present experiments, where fluorescein sulfonate is used, the filter cube consists of a 512-nm longpass dichroic mirror and the usual 520-nm fluorescein cut-on filter (*F1*). The proper wavelength for DIC optics is selected with a narrow 512-nm bandpass filter (*F2*) in the transmitted light path above the condenser. The filters were supplied and tested by Omega Optical, Inc. (Brattleboro, VT). Instead of the usual fixed quarter waveplate for circular polarization, our DIC system includes a liquid crystal variable wavelength retarder (Model 1020, Meadowlark Optics, Longmont, CO), which enables complete remote control of polarization state. DIC images are obtained at low intensifier gain.

In vitro microperfusion of tubules

Terminal inner medullary collecting duct (IMCD) segments were dissected from the last two thirds of the renal inner medulla of male Sprague-Dawley rats (Small Animal Breeding Facility, National Institutes of Health, Bethesda, MD). The isolated tubules were perfused in vitro at 37°C using glass micropipettes as previously described (Flamion and Spring, 1990). Our double-bath chamber allows observation of the perfused tubule at high magnification and provides laminar flow bath exchange without movement of the tubule (Strange and Spring, 1986). Perfusion was driven by hydrostatic pressure, and fluid was collected at the distal end of the tubule with a calibrated volumetric pipette. The IMCD segments were bathed in CO_2-gassed isotonic Ringer made up of (in mM): 124 Na, 25 $NaHCO_3$, 2.5 K_2HPO_4, 1.2 $MgSO_4$, 2.0 $CaCl_2$, 5.5 glucose, and 5.0 urea. The perfusate was prepared freshly by adding fluorescein sulfonate 800 μM (FS; Molecular Probes Inc., Eugene, OR) to the bath solution. Illumination was always used sparingly to avoid photodamage.

Fluorescein sulfonate was selected as the fluorophore because (*a*) its peak excitation wavelength is $\approx$490 nm (Chen et al., 1988; Kuwahara et al., 1988), corresponding to the strong 488-nm line of the argon laser; (*b*) it is membrane impermeant in collecting ducts and therefore can be used as a luminal volume tracer (Kuwahara et al.,

1988); and (*c*) its fluorescence is relatively insensitive to pH > pH 7.0 (Chen et al., 1988). Preliminary experiments showed that a freshly made, well-oxygenated FS solution would bleach readily. Shot noise was reduced, and bleaching efficiency was improved, by raising the dye concentration >500 μM, but, under our experimental conditions, fluorescence intensity became slightly nonlinear with respect to FS concentration at concentrations >1500 μM. Although quenching has been reported to occur only at concentrations >3 mM under similar conditions (Chen et al., 1988; Kuwahara et al., 1988), other phenomena, such as an inner filter effect, may be responsible for that nonlinearity. Accordingly, to ensure a linear, low-noise response, 800 μM was selected as the concentration of FS in the perfusate.

Typical experiment

The entire experiment is computer controlled, using an IBM PC/AT and customized software. With the isolated perfused tubule held straight and horizontal as close as possible to the bottom of the chamber, the microscope focus is adjusted to coincide with the midplane of the lumen. The region illuminated by the laser light is limited by the rectangular image of the slit diaphragm projected in the plane of focus (Fig. 2). The length of the slit, L, is usually set to ≈75 μm, and the width to 40 μm, so that it completely overlaps a portion of the tubule. Because fluorescein sulfonate is cell impermeant, fluorescence will be emitted only from the luminal region, as confirmed by fluorescence images of the tubule taken at various times. Background fluorescence, including autofluorescence from tubular cells, was always <1% and remained unchanged after photobleaching. It was thus omitted from the calculations.

A typical experiment consists of the following steps (Fig. 3): laser light is turned on at low power and the emitted fluorescence is recorded during a baseline period of counting (100 data points). Then, the optical shutter in front of the photomultiplier tube is closed, and a bleach pulse of specified duration (usually 20 ms) is produced by suddenly switching the laser light to maximum intensity with the acousto-optic modulator. The bleaching light creates a reproducible pattern of reduced fluorophore concentration within the illuminated region. The reverse operation is performed to monitor fluorescence recovery. The first three points (1.5 ms) after the end of the bleach pulse are discarded to account for the rise-time of the optical shutter. Fluorescence recovers to its prebleach level as new unbleached molecules flow into the observation region. Computer software displays the time course of fluorescence recovery, from which fluid velocity is calculated as discussed later. Note that total exposure to laser light is limited to 1 s. DIC images of the tubule are recorded twice, at the beginning and at the end of each run, to yield accurate measurements of inner tubule diameter.

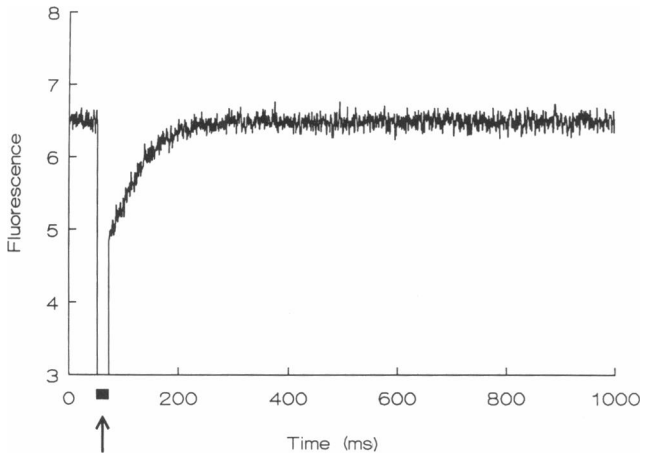

FIGURE 3 Typical FPR experiment in an isolated tubule perfused with a fluorescein sulfonate solution. Fluorescence is measured as the amplified photomultiplier current. Data are not smoothed. During the 20-ms bleach pulse, indicated by the arrow, the laser light intensity is suddenly increased 500-fold, and the photomultiplier is shut off by an electro-optic shutter.

THEORETICAL ANALYSIS AND CONTROLS

The aim of data analysis in any FPR experiment is to determine the mobility of unbleached fluorescent molecules from the rate at which they replace the bleached particles in the illuminated region. The typical spot FPR technique, which is used mostly to measure diffusion coefficients in thin samples, employs a focused laser beam and resorts to a narrow aperture in an image plane in front of the photomultiplier to reduce the effective depth-of-field for fluorescence collection (Wolf, 1989). These prerequisites allow a two-dimensional treatment of fluorescence recovery, with diffusion or flow confined to a infinite plane coincident with the focal plane of the microscope objective (Axelrod et al., 1976). Generally, the spatial variation in light intensity within the plane is Gaussian.

In the present experiments, the situation is different because (*a*) illumination is approximately uniform, as discussed later, (*b*) fluorescence is emitted only from a finite volume (the tubule lumen bounded by the observation window), (*c*) the recovery mechanism, steady laminar flow, is unidirectional, and (*d*) partial recovery occurs during the bleaching interval. These issues underlie the theoretical analysis outlined below.

Velocity profile

The illumination and fluorescence collection geometries are schematized in Fig. 2. Because steady flow that is due to pressure drop along the tubule can be modeled as Poiseuille flow in a small cylindrical tube, the perfusate velocity profile is parabolic in the radial coordinate, ρ:

$$v(\rho) = 2v_m\left[1 - \left(\frac{\rho}{\rho_i}\right)^2\right], \quad (1)$$

where ρ_i is the inner tubule radius and v_m, the mean axial velocity, is given by:

$$v_m = Q/A = Q/\pi\rho_i^2, \quad (2)$$

with Q being the volumetric flow rate and A, the luminal cross-sectional area. In a typical experiment, $\rho_i \approx 12.5$ μm and Q varies from 4 to 40 nl/min, so v_m will range from 0.014 to 0.14 cm/s. The Reynolds number can be calculated as $Re = 2\rho_i v_m/\nu$, in which the kinematic viscosity, $\nu = 0.007$ cm^2/s. The low Reynolds numbers (range, 0.005–0.05) corroborate laminar flow conditions.

Theoretical analysis of fluorescence recovery

Only the essential steps in the derivation of expressions for fluorescence recovery over time are presented here; the details are summarized in the Appendix.

The analysis includes two major assumptions: that bleaching of the fluorophore is a first-order photochemical reaction with a rate constant k, and that the excitation light intensity is approximately uniform over the observation region. Both assumptions were tested experimentally and the results are discussed in detail later. For now, let us mention that the first assumption was shown to be valid and that deviations from the second were reckoned to be <7%.

For analytical convenience, $t = 0$ is defined as the beginning of the bleach pulse. Fluorescence recovery, expressed in fractional form, is defined as:

$$f_R(t) = [F(t) - F_0]/[F_\infty - F_0], \quad (3)$$

where $F(t)$, F_0, and F_∞ are the fluorescences at time t, at the beginning of the recovery phase ($t = t_b + t_s$), and after complete recovery, respectively. The time intervals, t_b and t_s, are the durations of the bleach pulse and shutter response, respectively.

As demonstrated in the Appendix and illustrated in Fig. 4, $f_R(t)$ increases linearly with time from $t = t_b + t_s$ to $t = L/2v_m$, where L is the length of the illuminated region. During that period, as new unbleached dye flows into the observation region, all dye exiting the region has been "maximally" bleached (that is, exposed to bleaching light for a time t_b); hence fractional recovery is linear with respect to time. At $t = L/2v_m$, indicated by the dotted line in Fig. 4, dye that is less than maximally bleached begins to exit the observation region, thus causing the rate of recovery to slow. The proportion of bleached fluorophore in the exit stream decreases until, at complete recovery, all of the bleached fluorophore has been washed away. The strict upper limit for linearity, expressed by the range of center line transit times, $L/2v_m$, was 28–280 ms for the range of flow rates measured in the present experiments. However, the

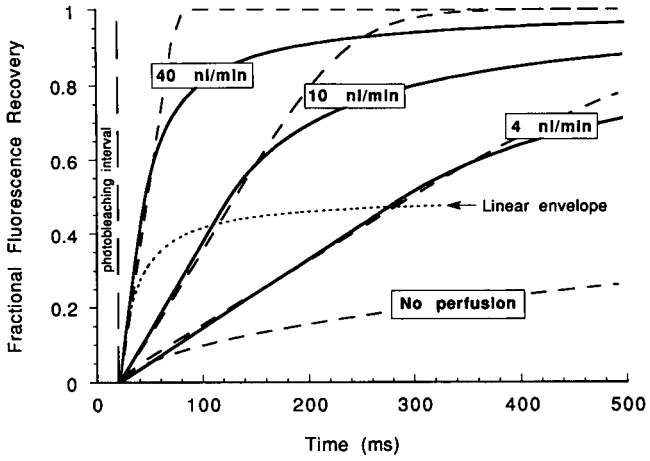

FIGURE 4 Simulated fractional fluorescence recovery, $f_R(t)$, for different axial flow rates in an isolated perfused tubule based on two mathematical models: (*a*) parabolic flow without diffusion at 4, 10, and 40 nl/min (*solid curves*), and (*b*) plug flow with diffusion at 0, 4, 10, and 40 nl/min (*dashed curves*). Strictly linear increases in recovery are only predicted by the parabolic flow model within the envelope indicated by the dotted line. However, both models yield similar, nearly linear, predictions over longer intervals within the practicable flow rate range of 4–40 nl/min. Parameter values used were ρ_i (inner radius) = 12.5 μm, L (length of the illuminated region) = 75 μm, t_b (bleach time) = 20 ms, t_s (shutter interval) = 1.5 ms, and k (bleaching coefficient) arbitrarily set to correspond to ≈25% bleach (see text).

recovery curves are nearly linear for significantly longer intervals, particularly at the higher flow rates.

The linear portion of $f_R(t)$ is described by:

$$f_R(t) = \frac{(v_m/L)(t - t_b - t_s)}{1 - (v_m t_s/L) - (v_m t_b/L) \times \dfrac{1 - (1 + kt_b)\,e^{-kt_b}}{kt_b(1 - e^{-kt_b})}}. \quad (4)$$

For $kt_b \ll 1$, Eq. 4 can be simplified, and the slope of the $f_R(t)$ plot can be expressed as:

$$\text{slope} \approx \frac{v_m/L}{1 - (\tfrac{1}{2}t_b + t_s)(v_m/L)}. \quad (5)$$

Rearranging,

$$v_m \approx L/(\text{slope}^{-1} + \tfrac{1}{2}t_b + t_s). \quad (6)$$

For our usual experimental conditions, i.e., $\rho_i = 12.5$ μm, $L = 75$ μm, $t_b = 20$ ms, $t_s = 1.5$ ms, and $kt_b \leq 0.3$ (the latter corresponds to ≈25% bleaching, the maximum bleaching achieved in the present experiments), the above approximation is accurate to within 0.1% for the slowest flow rates (4 nl/min), and to within 1.25% for the fastest flow rates (40 nl/min). Note that this

simplified solution for v_m does not contain the bleaching rate coefficient, k, and hence is insensitive to the choice of fluorophore or to the factors that affect bleaching rate, which may vary from day to day, such as oxygen levels. Eq. 6 was used in the curve-fitting procedure to analyze experimental data.

For $t > L/2v_m$, $f_R(t)$ is nonlinear with respect to time according to Appendix Eqs. A7 and A8.

Before presenting the experimental results, let us first discuss the major assumptions underlying the theoretical analysis presented above.

Influence of diffusion and shape of the velocity profile

In principle, recovery and the removal of bleached fluorophore cannot be accomplished solely by convection; diffusion must play a role. The contribution of diffusion can be appreciated by calculating the Péclet number, defined as Pé $= v_m d/D$, where d is the inner tubule diameter and D is the diffusion coefficient of FS in aqueous buffer at 37°C. The values $d = 25$ μm, and $D = 7 \times 10^{-6}$ cm^2/s, which is a conservative estimate based on the Stokes-Einstein equation, yield Pé = 5–50 for the above-mentioned range of flow rates. Within this Pé range, convection is likely to dominate over diffusion in determining dye movement and hence recovery. The increasing importance of diffusion at lower flow rates is illustrated in Fig. 4 by the curve for "no perfusion" representing the recovery when the perfusate solution is stagnant. This curve and the other dashed curves in Fig. 4 were generated from an alternative model derived in the Appendix which considers dye diffusion in combination with the hypothetical constraint that the perfusate velocity is uniform everywhere within the tubule (plug flow) and equal to v_m. In contrast to the significant contribution of diffusion to recovery at zero flow, neither diffusion nor the shape of the velocity profile have much influence on the linear portion of recovery for flow rates of 4 nl/min and greater. In the nonlinear portion, the bleached dye is swept out of the observation too rapidly because of the unrealistic plug flow velocity profile, thus yielding steeper recovery curves than for the parabolic flow model.

Characterization of photobleaching

Axelrod and co-workers' canonical presentation of FPR data analysis (Axelrod et al., 1976) assumed that the photochemical reaction that bleaches the fluorophore is a first-order irreversible reaction with a rate constant, k, proportional to the intensity of incident irradiation. Then, during the bleaching phase, the concentration of unbleached fluorophore at position x and time t $[C(x, t)]$ can be described as:

$$\frac{dC(x,t)}{dt} = -k(x) \times C(x,t), \qquad (7)$$

where the rate constant, $k(x) = \alpha I(x)$, in which α is a photochemical quantum yield and $I(x)$ is the bleaching light intensity profile in the specimen. This important assumption, however, has rarely been tested experimentally. Kapitza and Sackmann (1980), using erythrocyte ghost membranes, and Lanni et al. (1981), with bulk solutions of FITC-dextrans, demonstrated first-order bleaching kinetics and a linear relation between local rate constants, $k(x)$, and $I(x)$. Experiments in cells, on the other hand, have revealed a loss of first-order kinetics at the highest light intensities (Benson et al., 1985).

To determine the time course of FS photolysis, we used a very thin film of immobile fluorophore, equivalent to a single plane. Because the illumination profile in the focal plane was uniform (see Methods and Fig. 7), flourescence, as integrated by the photomultiplier, directly reflected fluorophore concentration, $C(x, t)$. A fresh FS solution, embedded in epoxy to prevent diffusion, was compressed between two coverslips and was placed on the microscope stage at the position of the bottom of the chamber. The sample was exposed to various laser light intensities, ranging from the usual monitor intensity, when no significant bleaching was detected, to the maximum intensity used for the bleach pulse (Fig. 5). All curves could be well fit to the single exponential solution to Eq. 7. Moreover, bleaching coefficients, k, extracted from these curves were linearly related to light intensity. We also verified that photobleaching was indeed an irreversible reaction (Fig. 5, *inset*). The relationship between k and light intensity was tested more thoroughly at 37°C using a thin layer of freely diffusible FS solution, which is closer to the experimental conditions of tubule perfusion but yields more limited information because lateral diffusion progressively obscures the curves of fluorescence decay. Even so, there was a close linear correlation between initial bleaching coefficients and light intensity (Fig. 6).

Spatial variations in light intensity

The theoretical analysis presented above assumes that excitation light intensity and bleaching are independent of radial position in the tubule. Because we use a high N.A. objective lens (see Discussion), implying divergence of the exciting light beam above and below the focal plane (see Fig. 2), this prerequisite is not entirely true. However, the cylindrical geometry of the specimen tends to attenuate that potential error. To test this issue

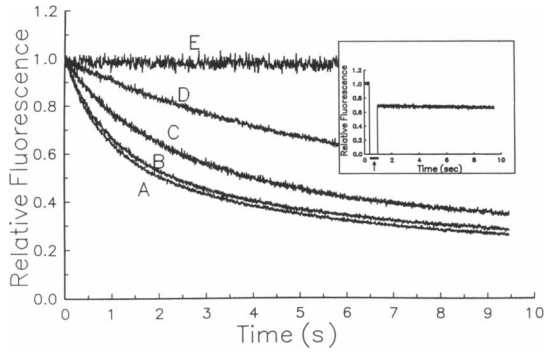

FIGURE 5 Characterization of photobleaching. Fluorescence decay of immobile, nondiffusible samples of fluorescein sulfonate (FS) exposed to various laser light intensities. FS is embedded in epoxy glue to prevent diffusion. Data are normalized to the initial values. Curve *A* is obtained with the maximum bleaching light intensity (100%). Curves *B* to *D* correspond to 78%, 50%, and 28% light intensity, respectively. Curve *E*, the result of monitor light intensity (0.2%), discloses no photobleaching. Curves *A* to *D* could be fitted ($r^2 > 0.98$) to a single exponential of the form: $y = 0.25 + 0.75e^{-kt}$, where 0.25 is the unbleachable fraction probably due to the unusual structure of the dye-epoxy combination (a droplet of FS solution will bleach almost entirely and with a faster time course). Bleaching coefficients k were linearly related to light intensity ($r^2 > 0.99$; not shown). (*Inset*) Fluorescence emitted from a similar nondiffusible sample observed with monitor light intensity before and after a 600-ms bleach pulse (indicated by the *arrow*) produced by maximum light intensity. The absence of fluorescence recovery signals irreversible photobleaching.

experimentally, the volume of luminal fluid in the illuminated region of a 25-μm-diameter tubule was modeled as a stack of optical sections perpendicular to the optical axis, with the focal plane, which receives the

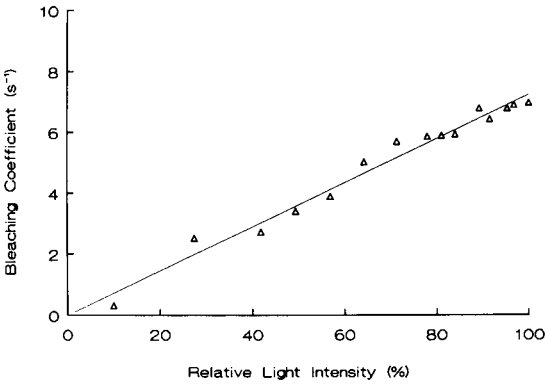

FIGURE 6 Relation between light intensity and bleaching coefficients for immobile but freely diffusible samples of FS solution at 37°C. The samples were exposed to various laser light intensities expressed here in % of maximum bleaching light intensity. For each light intensity, a bleaching coefficient was calculated by fitting to a single exponential the first 50 ms of fluorescence decay. The least-square linear regression (*solid line*) is given by: $y = -0.007 + 0.072 \times (r^2 = 0.97)$.

maximum irradiance, coincident with the midplane of the tubule (Fig. 2). The model system for simulating the optical sections through the tubule consisted in a 1-μm-thick, uniform layer of 1% eosin. This film was epi-illuminated through the rectangular slit diaphragm used in the tubule experiments. A very low light flux was used to avoid any photolysis. The plane of focus was then moved along the optical axis in 1.2-μm increments relative to the film. A fluorescence image captured with the intensified CCD camera was recorded at each position. With the aid of an image processing software package (Image-1, Universal Imaging Corp., West Chester, PA), the area of the corresponding luminal section was traced on the image at each step (Fig. 7). The average fluorescence per luminal section, measured from the area brightness after checking for linearity in the gray scale, reflects the relative light intensity delivered to each section of the model tubule, but also includes the fluorescence collection efficiency of the optical system. As shown in Fig. 7, average fluorescence decreased moderately with distance from the plane of focus, reaching a minimum value of 77% at the position farthest from the objective (+12 μm). The small asymmetry with respect to the focal position may have been due to a better fluorescence collection efficiency for the planes closer to the objective (negative values on the optical axis).

Because the out-of-focus regions of the lumen were irradiated with less intensity, the contribution of the midplane fluorescence to the signal recorded by the photomultiplier during the flow experiments was somewhat overweighted, and v_m calculated according to Eq. 6 might have been overestimated (If the thickness of the illuminated [and bleached] midplane layer of fluorophore is $\ll$ tubule radius, one can show that the solution for v_m according to Eq. 6 simply has to be multiplied by 0.75). However, integrating the collected fluorescence values of Fig. 7 into a cylindrical model of the tubule disclosed a loss of signal of only 7.4% compared to a homogeneously illuminated tubule. In addition, the glass tube calibration experiments, described below, did not suggest any systematic bias in the determination of v_m. The fluorescence images of Fig. 7 also revealed that a small amount of out-of-focus luminal solution outside the observation window, i.e., upstream and downstream, was illuminated as well. From brightness measurements and three-dimensional modeling, that portion was estimated to be $\approx 5\%$ of the total luminal volume illuminated; its contribution would counterbalance the decreased signal from the out-of-focus sections of the tubule. Because these opposite effects due to the expanded light beam were small compared to the total

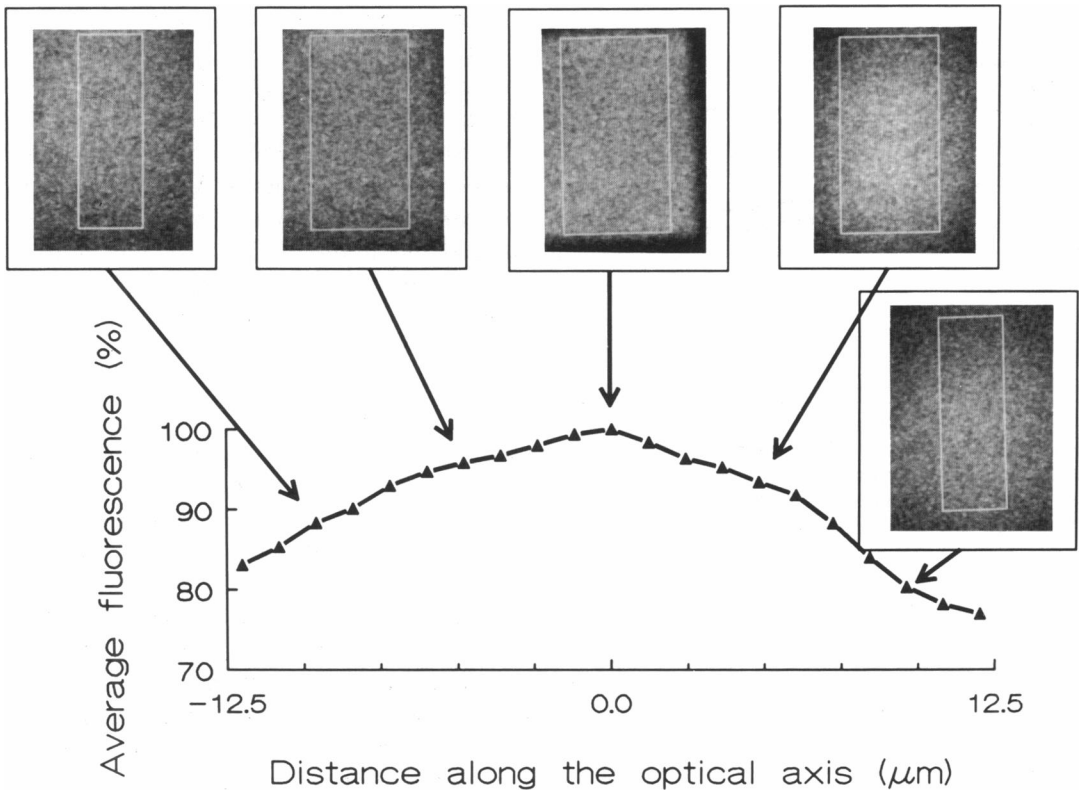

FIGURE 7 Evaluation of the light intensity delivered to various sections of a 25-μm diameter model tubule (see Fig. 2). To simulate optical sections (perpendicular to the optical axis) through the tubule, the microscope focus is moved in 1.2-μm steps relative to a 1-μm thick, uniform film of eosin. An intensified fluorescence image is recorded at each position. The focal plane coincides with the film at zero; negative values denote the planes closer to the objective. At each step, the area corresponding to a luminal section through the model tubule, bounded by the length of the rectangular slit diaphragm, is traced on the image. Five such sections, located at −9.6, −4.8, 0, +4.8, and +9.6 μm are shown in the insets. The average fluorescence per luminal section, plotted on the *y*-axis as a percentage of the fluorescence at zero, expressed the relative light intensity delivered to each section of the tubule, together with the fluorescence collection efficiency of the optical system (see text).

fluorescence, no attempt was made to include them in the theoretical data analysis.

The expected spatial distribution of photobleaching, based on the same model, is depicted schematically in Fig. 8, which represents the amount of unbleached fluorophore left in every section of the tubule after a 30-ms bleach pulse in the absence of flow. The level of bleaching in each section was calculated from (*a*) the relative light intensity measurements of Fig. 7, (*b*) the linear regression line of Fig. 6, which predicts the bleaching coefficient, k, for each light intensity, and (*c*) the formula:

$$F_{\text{post-bleach}} = F_{\text{pre-bleach}} \times e^{-kt_b}, \quad (8)$$

which derives from Eq. 7. In Fig. 8, this experimentally determined bleach profile is compared to a theoretical, spatially uniform 20% bleaching. The integrated difference between the calculated experimental bleaching and uniform bleaching is 1.9% of all unbleached fluorophore. In conclusion, despite divergence of the light beam, the assumptions of uniform illumination and photobleaching over the observation region appear to be reasonable.

EXPERIMENTAL RESULTS

Data analysis

The computer program for calculating the mean fluid velocity, v_m, first converted the fluorescence recovery data to fractional form, $f_R(t)$, according to Eq. 3. F_∞ was taken as the mean of the last 100 data points. F_∞, as expected, was always identical to the prebleach florescence. F_0 was the fluorescence at $t = t_b + t_s$, with the bleach time, t_b, = 20 or 30 ms, and the finite switching time, t_s, = 1.5 ms. A least-square linear regression

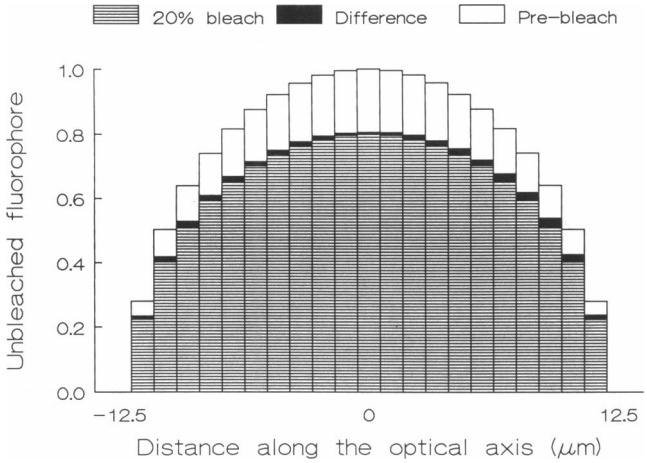

FIGURE 8 Theoretical plot of photobleaching in a model tubule (assuming no flow), employing experimentally determined values of the bleaching coefficients, k. The bars represent the relative amounts of unbleached fluorophore in various discrete sections of a 25-μm diameter model tubule centered in the focal plane (zero along the optical axis). The total height of the bars indicates the theoretical distribution of fluorophore before the bleach, i.e., the luminal volume. The striped portions of the bars display the result of a spatially uniform 20% bleach. The black rectangles represent the difference between this uniform bleaching and the expected result of a typical 30-ms bleach pulse which reduced the amount of fluorophore at the midplane by ≈20%. The actual amount of bleaching in each section has been calculated using the experimentally determined k's from Fig. 6 and the spatial distribution of light shown in Fig. 7 (for more details, see text).

analysis, starting at F_0 and including at least 20 data points, was performed. V_m was calculated from the slope of this line using Eq. (6). Care was taken to remain in the linear portion of the fractional recovery curve, although, at the highest flow rates, the error incurred by extending the linear regression analysis slightly beyond $t = L/2v_m$ would be negligible, as denoted in Fig. 4.

Axial flow rate is the product of v_m and cross-sectional area of the tubular lumen. The latter was calculated from the mean luminal diameter measured by tracing the DIC images of the tubule recorded at the beginning and at the end of each run. Luminal diameters never changed significantly during that period.

Calibration experiments

To first test the accuracy of data analysis as described above, a series of flow rate calibration experiments were performed using glass capillary tubes designed to mimic the perfused tubules. Glass capillaries (Drummond Scientific Co., Bromall, PA) were pulled on a microforge to an inner diameter approximately equal to that of a perfused terminal IMCD segment (20–25 μm). They were glued onto a coverslip, mounted on the microscope stage, connected by stainless steel tubing to a carefully calibrated nanoliter pump (Model 1400 EC, World Precision Instruments Inc., New Haven, CT), and perfused with the same FS solution at predetermined flow rates (10–40 nl/min). Tubules and glass tubes were observed under strictly identical conditions.

As shown in Table 1, there was an excellent correlation between the flow rates imposed by the pump in the glass tubes and their experimental determinations using FPR. The mean coefficient of variation was 8.7% (n = 55 measurements).

Volume flow rates in microperfused tubules

Four rat terminal IMCD segments, 430–995 μm long between perfusion and collection holding pipettes, were perfused at various flow rates by adjusting the hydrostatic pressure. Fluid was collected at the distal end of the tubles using volumetric pipettes. During each timed fluid collection, which lasted from 42 s to 18 min, 22 s, 1–6 flow rate measurements by the FPR method were made. Three typical curves of fractional fluorescence recovery, obtained in the same tubule at three different flow rates, are displayed in Fig. 9. The results of 66 flow rate measurements in four perfused tubules are summarized in Fig. 10. There is an excellent correlation (r^2 = 0.97) between the FPR measurements and the flow rates determined by the fluid collection method, especially if one considers that the latter is a time integral of the FPR measurements. Also note that FPR measurements can be performed at various axial positions along the tubule without introducing any obvious bias (Fig. 10, *inset*).

TABLE 1 Flow rate measurements in perfused glass tubes by the FPR method

Pump flow rate	Experimental flow rate measurements			
	n	Mean	SD	Range
		nl/min		
10	8	10.4	1.2	8.8–12.7
12.5	7	12.9	1.2	11.2–14.6
15	15	15.0	1.4	12.1–17.7
20	5	21.2	1.4	19.6–22.7
25	8	24.7	1.7	22.5–28.1
30	5	31.2	2.6	28.3–34.8
40	7	39.3	2.9	35.1–43.2

Flow rates are controlled by a calibrated nanoliter pump. n = number of measurements.

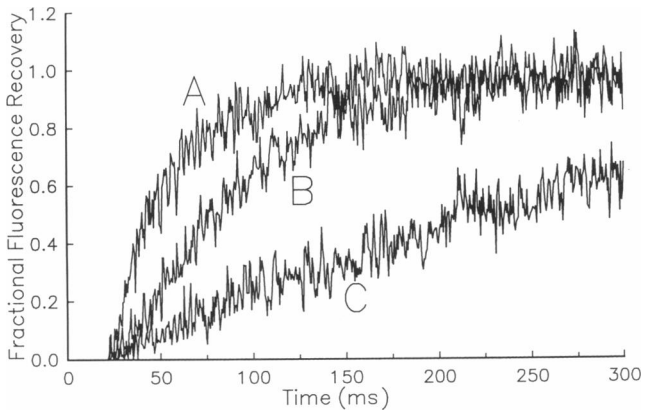

FIGURE 9 Typical curves of fractional fluorescence photobleaching recovery in a single tubule perfused at three different flow rates. Time is zero at the beginning of the bleach pulse. Flow rates measured by the FPR technique were (in nl/min): *A*, 40.37; *B*, 14.91; *C*, 6.23. The corresponding inner tubule diameters were 24.6, 24.0, and 23.6 μm.

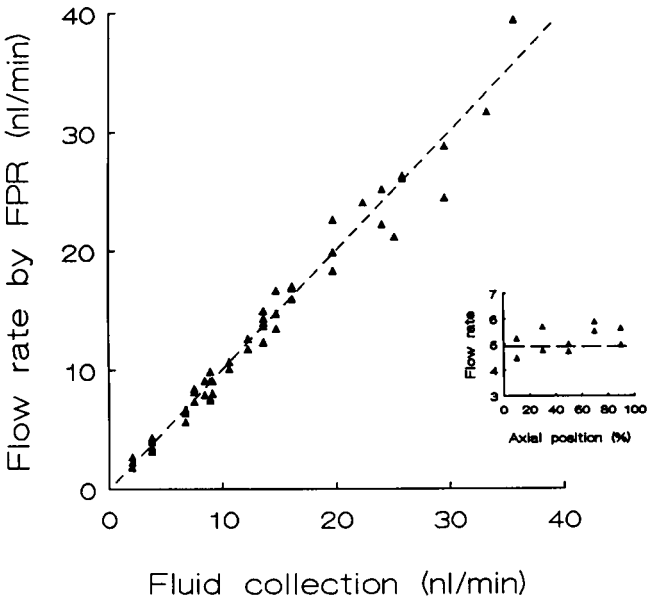

FIGURE 10 Comparison of perfusion flow rates determined by fluid collection and by the FPR method in isolated tubules perfused at various hydrostatic pressures. Each closed triangle represents a single FPR measurement ($n = 66$). One to six FPR measurements are performed during any given timed fluid collection. The dotted line is the line of identity. The least-square linear regression is given by: $y = 0.10 + 0.98x$ ($r^2 = 0.97$). (*Inset*) Flow rate determinations by the FPR method (*open triangles*) at various axial positions along the tubule during a single fluid collection period which yielded an integrated flow rate of 4.91 nl/min (indicated by the *dashed line*). Axial position is expressed in percent of the total perfused length, 0% being the tip of the perfusion pipet and 100%, the mouth of the distal holding pipet.

DISCUSSION

Flow rate measurements using the FPR technique exhibited excellent accuracy and reproducibility, as demonstrated by calibration experiments in small glass tubes perfused at predetermined flow rates. In microperfused kidney tubules, the method showed good correlation with the standard fluid collection procedure. A few methodological points, however, deserve comment, particularly with respect to the geometry of the experiments.

When FPR measurements are carried out in bulk solution samples, as opposed to fluorescently tagged plasma membranes, divergence of the exciting light beam above and below the plane of focus can introduce spatial variations in both the magnitude of bleaching and the efficiency of fluorescence collection. A common solution in such cases has been to use a relatively low N.A. objective lens and to focus the laser beam onto the specimen, thereby assuming a uniform beam radius throughout the sample, whether solution of fluorophore (Jacobson et al., 1976; Lanni et al., 1981), cytoplasm (Wojcieszyn et al., 1981; Salmon et al., 1984), or tissue interstitium (Chary and Jain, 1989). Moreover, diffusion coefficients can be measured in bulk solutions using a high N.A. lens and a focused laser beam, because the contribution of motion in the direction of the optical axis is negligible provided the beam radius is $\ll$ specimen thickness (Icenogle, 1981). Measuring flow rates in perfused tubules, however, imposes different constraints. Both a high N.A. objective lens and a large field of view were found necessary for two reasons. First, low N.A. lenses reduce the illuminance to the specimen and thus require bleach times that are too long for the fast flow rates we intended to measure. Second, the time resolution of the electronics circuit was insufficient to observe the extremely rapid washout of a small spot such as that produced by a focused laser beam. An additional reason to use high magnification was to achieve concurrent DIC microscopy of the tubular cells (Spring, 1990), which permits measurement of cell membrane water permeabilities and transepithelial fluid transport in a truly simultaneous manner (Flamion, B., C. C. Gibson, and K. R. Spring; in preparation).

We therefore decided to use a high N.A. objective lens filled with a uniform illuminating beam, and to limit the field of view with a rectangular fluid diaphragm. Uniform illumination was obtained by conveying the laser light to the microscope through a flexible light guide which was continuously vibrated (Ellis, 1979). (This solution is better than simply cutting off the wings of the Gaussian intensity profile of the laser beam by a field stop, as proposed by Kapitza and Sackmann [1980;

see also Peters, 1984]). Because of this optical arrangement, however, we could not easily predict the axial variations in light intensity, and possibly in the magnitude of photobleaching, throughout the specimen. We therefore devised a model system based on a three-dimensional model of the tubule, and used a thin film of fluorophore scanned along the optical axis. The results indicated that photobleaching was fairly insensitive to radial position in the tubule. Quasi-uniform bleaching, despite light beam divergence, results from the combination of first-order bleaching kinetics, short bleach times (20 ms), and cylindrical geometry of the tubule. There may be other ways to obviate the three-dimensional problem, such as using a lower N.A. objective lens together with a much more powerful laser, which would simplify the assumptions related to the distribution of light. Another solution, namely to reduce the collection of emitted fluorescence to a single plane by using appropriate diaphragms in the secondary image plane, was found unsuitable for the present experiment, given the requirement for a large illumination field. Laser scanning confocal microscopy, with its high axial resolution, may seem an elegant alternative (Wells et al., 1989), if it were not for its poor time resolution.

Fluorescence recovery in the isolated perfused tubules was analyzed with a fluid dynamics approach. Data analysis was restricted to the first part of the recovery curve, which is linear when expressed in fractional form. This has several important advantages: (*a*) Linearity can be expected even if the shape of the velocity profile in the tubule differs from an ideal parabola because the profile has not yet fully developed near the tubule inlet, or perfusate viscosity is non-uniform, or there are wall irregularities; (*b*) Diffusion can be omitted in the analysis. Dye diffusion occurring within the observation region will have little effect on fluorescence integrated by the photomultiplier. Diffusion into or out of the observation region should be negligible because the axial gradients remain small across the inlet and exit planes. (*c*) The flow rate determination is insensitive to the bleaching rate constant or the magnitude of bleaching. The latter can be adjusted, by varying the bleach time, to reach 20–25%, which satisfies the simplifying conditions of Eq. 6 while overcoming shot noise and other signal fluctuations.

Nevertheless, the linear portion of the fractional recovery curve shortens with higher fluid velocities. For data analysis, a practical requirement of more than 20 fluorescence values taken at 0.5-ms intervals demands a linear portion of at least 10-ms duration, which corresponds to a flow rate of the order of 40 nl/min in a 25-μm diameter tubule. To improve the accuracy of the method at these high flow rates, or to measure faster flow rates, the experimental data can be fitted over a longer period with a nonlinear regression analysis, although that would require enhanced computational facilities and could introduce new assumptions related to points (*a*) to (*c*) above.

Another advantage of the FPR method is the ability to measure flow rate at any axial position along the perfused tubule. A possible restriction concerns the entry length, ℓ, defined as the downstream distance from the tip of the perfusion pipette where the maximum velocity reaches 99% of the maximum velocity of the fully developed Poiseuille flow. In small cylindrical tubes with Reynolds numbers $\ll 1$, which also applies to the perfused tubules, $\ell \approx 1.3\ \rho_i$ (Lew and Fung, 1969), i.e., 12–17 μm in the present series. However, as noted in connection with Fig. 4, variation in the shape of the velocity profile should have little influence on the linear portion of the recovery curve.

Our experiments were performed in rat IMCD segments in the absence of an osmotic gradient, thus ruling out fluid absorption across the epithelium. However, physiologically relevant experiments in collecting ducts will often include transepithelial water reabsorption, with two possible consequences: a perturbation of the velocity profile, and a concentration polarization of the impermeant dye retained in the lumen. Both issues need to be addressed.

First, in the presence of transmural water loss which is nearly uniform over the length of the observation region, the parabolic axial velocity profile can be approximated by:

$$v_z(\rho) = [2v_m - 4v_w(z/\rho_i)][1 - (\rho/\rho_i)^2], \qquad (9)$$

in which ρ and z are the radial and axial coordinates (Fig. 2), v_z is the axial velocity within the lumen, and v_w is the radial flux across the tubule wall. For ρ_i (inner tubule radius) = 12.5 μm, and L (length of the illumination window) = 75 μm, the decrease in the mean velocity, $2(L/\rho_i)v_w$, $= 12v_w$. Within the present range of perfusate flow rates (4–40 nl/min), the transmural flux corresponding to a 5% decrease in flow rate between the inlet and outlet of the observation region ranges over $6 \times 10^{-5} - 6 \times 10^{-4}$ cm$^3 \cdot$ cm$^{-2} \cdot$ s^{-1}. In most collecting ducts, whose osmotic water permeability in the presence of antidiuretic hormone reaches $\approx 9 \times 10^{-4}$ cm $\cdot$ s$^{-1} \cdot$ kg $\cdot$ osmol^{-1} (Verkman, 1989), this amount of transmural water flux can be induced by an osmotic gradient of ≈70 mosm/kg H_2O at a perfusion flow rate of 4 nl/min, up to a gradient of ≈700 mosm/kg H_2O at 40 nl/min. Larger osmotic fluxes would introduce a >5% gradient in axial velocity within the observation region.

Second, if the dye is retained within the lumen, transepithelial water reabsorption will create some degree of polarization near the tubule wall, i.e., the

development of a spatially varying concentration profile adjacent to the wall. The magnitude of this effect can be approximated by the standard formula (Barry and Diamond, 1984):

$$C_w/C_b = e^{-v_w\delta/D}, \quad (10)$$

in which C_w and C_b are the fluorophore concentrations at the wall/lumen interface and in the bulk solution, respectively; D is the diffusion coefficient of FS taken as 7×10^{-6} cm^2/s, and δ is a characteristic thickness of the polarization or the unstirred layer. To generate a 5% radial gradient in concentration at the highest v_w, δ would have to be >50 μm, a physically impossible condition in perfused tubules.

A last point pertains to the question of photodamage, especially during the study of various physiological transport phenomena in perfused tubules. Photodamage is usually considered minimal in FPR experiments (Petersen et al., 1986), especially when exposure time and total irradiation does are minimized as in the present experiments. Furthermore, fluorophores were confined to the tubule lumen, where any harmful by-product of the bleaching process is expected to be washed away quickly. Nevertheless, during preliminary experiments, when exposure to laser light was not carefully controlled, some portions of the tubules developed localized wall thickening and loss of resilience. Local heating of the fluorophore solution by the bleaching light is not a likely cause, because conservative calculations based on equations derived by Simon et al. (1988) suggested a temperature transient of +2.2°K in the center of the irradiated volume, in the absence of heat loss by convection. Such brief heating should not be deleterious to the nearby tubular cells. Therefore, a direct effect of laser light on cell proteins seems more likely, which would dictate that bleach times and total irradiation times be kept as short as possible. When strictly limited to 1-s experiments with 20- or 30-ms bleach pulses, laser light exposure did not produce any observable deterimental effect, including any effect on transcellular water permeability measurements, after up to 30 successive flow rate determinations in the same tubule (unpublished observations).

As demonstrated in the present report, FRP can be used to measure fluid velocities of the order of 0.1 cm/s in small cylindrical tubes and kidney tubules. Combined with imaging assessment of the inner tubule diameter, the method provides an instantaneous measurement of flow rate at any axial position in kidney tubule segments perfused with an impermeant fluorophore, and is limited only by the available laser power and the speed of data acquisition. Similar tactics could be applied to the determination of flow rate in kidney tubules observed with intravital microscopy, or even in vasa recta and other blood capillaries. The presence of cells with different fluorescence properties from the plasma is likely to necessitate that measurements be made on cell-free interludes. To be impermeable in such vessels, the fluorophore may have to be associated with macromolecules. In situations of transmural loss of luminal fluid, the possibility of significant radial nonuniformity in the fluorophore would increase because of the lower diffusivity of macromolecules. Other possible confounding effects include temporal variations in the inflow concentration of fluorophore, binding between the fluorophore and mural constituents and endogenous sources of fluorescence.

APPENDIX

The fluorescence at time t during recovery, $F(t)$, as indicated by the photomultiplier tube current, can be related to the fluorophore concentration within the observation region, $C(\rho, z, t)$, and to the excitation light intensity profile, $I_r(\rho, z)$, by the integral:

$$F(t) = 2\pi \int_0^L \int_0^{\rho_i} q_r I_r(\rho, z) C(\rho, z, t) \rho d\rho dz, \quad (A1)$$

in which ρ and z are the radial and axial coordinates defined in Fig. 3, ρ_i is the inner tubule radius, and q_r represents the combined effects of absorption of exciting light by the fluorophore, fluorescence quantum efficiency, collection efficiency of the optical system, and conversion from rate of incident photons to output current by the electronics.

To simplify the evaluation of the integral in Eq. A1, let us assume that during a recovery interval q_r is independent of time and fluorophore concentration, and I_r is constant and uniform over the observation region. We apply the same assumptions to the preceding bleaching interval (and the corresponding q_b and I_b values), together with the assumption of irreversible, first-order bleaching kinetics described by the text Eq. 7 which contains a bleaching rate constant, k. Let $t = 0$ and $t = t_b$ correspond to the beginning and end of the bleaching interval, respectively, and $t = t_b + t_s$ correspond to the time at which the first fluorescence measurement is recorded after the electro-optic shutter is opened.

Recovery for parabolic flow in the absence of diffusion

The perfusate along the tubule axis is traveling at a velocity $2v_m$ according to Eq. (1). Because L is the length of the observation region, the fluorophore entering this region on the axis at $t = 0$ will exit the region at $t = L/2v_m$. During the time interval $t_b + t_s \le L/2v_m$, the fluorophore concentration in this region will vary as:

$$C(\rho, z, t) = \begin{cases} C_\infty, & \text{for } 0 \le z \le (t - t_b)v(\rho) \\ C_\infty \exp[-k\{z/v(\rho) - t + t_b\}], & \text{for } (t - t_b)v(\rho) < z \le tv(\rho) \\ C_\infty e^{-kt_b}, & \text{for } tv(\rho) < z \le L \end{cases} \quad (A2)$$

for all radial positions, $0 \le \rho \le \rho_i$. In the above C_∞ is the concentration of unbleached fluorophore.

The substitution of Eq. A2 into Eq. A1 leads to:

$$F(t) = \pi\rho_i^2 L q_r I_r C_\infty \times \left\{\frac{v_m(t-t_b)}{L} + \frac{v_m}{kL} \times (1 - e^{-kt_b}) + \left(1 - \frac{v_m t}{L}\right) e^{-kt_b}\right\}. \quad \text{(A3)}$$

The constants q_r, I_r, and C_∞ can be eliminated by expressing the result in the form of the fractional recovery defined by:

$$f_R(t) = \frac{F(t) - F(t_b + t_s)}{F_\infty - F(t_b + t_s)}, \quad \text{(A4)}$$

in which F_∞ is the fluorescence after complete recovery,

$$F_\infty = \pi\rho_i^2 L q_r I_r C_\infty. \quad \text{(A5)}$$

Combining Eqs. A3–A5 yields:

$$f_R(t) = \frac{(v_m/L)(t - t_b - t_s)}{1 - (v_m t_s/L) - (v_m t_b/L) \times \dfrac{1 - (1 + kt_b)e^{-kt_b}}{kt_b(1 - e^{-kt_b})}} \quad \text{(A6)}$$

which is Eq. 4 in the text. As noted there, Eq. A6 exhibits a linear increase in fractional recovery during the time interval $t_b + t_s \le t \le L/2v_m$.

By appropriate modification of the limits of the ρ and z intervals, Eq. A2 can be used to describe the fluorophore concentration within the observation region for times greater than $L/2v_m$. Combining the modified forms of Eq. A2 with Eq. A1, A4, and A5 leads to the following expressions for the fluorescence in the interval $L/2v_m \le t \le L/2v_m + t_b$,

$$F(t) = \pi\rho_i^2 L q_r I_r C_\infty \times \left\{\frac{v_m(t-t_b)}{L} + \frac{v_m}{kL} + \left(\frac{1}{2} - \frac{v_m}{kL}\right) \exp\left[-\frac{kL}{2v_m} + k(t-t_b)\right] - \left(\frac{kL}{4v_m}\right) e^{k(t-t_b)} \times \left[E_1\left(\frac{kL}{2v_m}\right) - E_1(kt)\right]\right\}, \quad \text{(A7)}$$

and for $t \ge L/2v_m + t_b$,

$$F[t] = \pi\rho_i^2 L q_r I_r C_\infty \times \left\{1 - \frac{kL}{4v_m} e^{k(t-t_b)} \times (E1[k(t-t_b)] - E1[kt])\right\}, \quad \text{(A8)}$$

in which $E_1(kt)$ is the value for kt of the exponential integral defined by

$$E_1(kt) = \int_{kt}^{\infty} \frac{e^{-x}}{x} dx \quad \text{(A9)}$$

Tabulated values of this integral can be found in handbooks, e.g., Abramowitz and Stegun (1965).

Recovery for plug flow with axial diffusion

The perfusate is assumed to flow axially with a velocity everywhere equal to the mean velocity, v_m. This is not a realistic assumption, but it tests the sensitivity of the recovery to shape of the velocity profile by comparison with the result for the parabolic representation of Eq. 1. We further simplify the analysis by letting the bleaching be instantaneous so that at $t = t_b$, the concentration is described by,

$$C(z, t_b) = \begin{cases} C_\infty, & \text{for } z < 0 \text{ and } z > L \\ C_\infty \exp(-kt_b), & \text{for } 0 \le z \le L. \end{cases} \quad \text{(A10)}$$

By replacing the fixed axial coordinate, z, with the coordinate, ζ, whose origin moves at velocity $v_m t$, defined by,

$$\zeta = -\frac{L}{2} + z - v_m(t - t_b), \quad \text{(A11)}$$

we can describe the changes in the concentration profile for $t > t_b$ by the diffusion equation,

$$\frac{\partial C}{\partial t} = D \frac{\partial^2 C}{\partial \zeta^2}, \quad \text{(A12)}$$

in which D denotes the dye diffusion coefficient. The solution to Eqs. A10–A12 can be obtained from Eq. 2.15 of Crank (1956) as,

$$C(\zeta, t) = C_\infty \left\{1 - \frac{1}{2}[1 - e^{-kt_b}] \times \left[\operatorname{erf}\left(\frac{\frac{L}{2} - \zeta}{2\sqrt{D(t - t_b)}}\right) + \operatorname{erf}\left(\frac{\frac{L}{2} + \zeta}{2\sqrt{D(t - t_b)}}\right)\right]\right\}. \quad \text{(A13)}$$

In the above, erf represents the error function described in Abramowitz and Stegun (1965). The substitution of Eq. A13 into Eq. A1 leads to Eq. A14 for the fluorescence behavior for $t > t_b$,

The fractional recovery is then obtained by combining Eqs. A4 and A14.

$$\frac{F(t)}{L\pi\rho_i^2 q_r I_r C_\infty} = \left\{1 - \frac{1}{2}[1 - e^{-kt_b}] \times \left[2\sqrt{\frac{D(t-t_b)}{\pi L^2}}\left[\exp\left(-\frac{(L - v_m[t-t_b])^2}{4D(t-t_b)}\right) - 2\exp\left(-\frac{v_m^2(t-t_b)^2}{4D(t-t_b)}\right) + \exp\left(-\frac{[L + v_m(t-t_b)]^2}{4D(t-t_b)}\right)\right] + \left[1 - \frac{v_m(t-t_b)}{L}\right] \operatorname{erf}\left(\frac{L - v_m(t-t_b)}{2\sqrt{D(t-t_b)}}\right) - \frac{2v_m(t-t_b)}{L} \operatorname{erf}\left(\frac{v_m(t-t_b)}{2\sqrt{D(t-t_b)}}\right) + \left[1 + \frac{v_m(t-t_b)}{L}\right] \operatorname{erf}\left(\frac{L + v_m(t-t_b)}{2\sqrt{D(t-t_b)}}\right)\right]\right\}. \quad \text{(A14)}$$

We wish to thank Raymond Mejia for his useful suggestions.

Received for publication 1 March 1991 and in final form 12 July 1991.

REFERENCES

Abramowitz, M., and I. A. Stegun. 1965. Handbook of Mathematical Functions. Dover Publications, Inc., New York.

Axelrod, D., D. E. Koppel, J. Schlessinger, E. Elson, and W. W. Webb. 1976. Mobility measurement by analysis of fluorescence photobleaching recovery kinetics. *Biophys. J.* 16:1055–1069.

Barry, P. H., and J. M. Diamond. 1984. Effects of unstirred layers on membrane phenomena. *Physiol. Rev.* 64:763–872.

Benson, D. M., J. Bryan, A. L. Plant, A. M. Gotto, Jr., and L. C. Smith. 1985. Digital imaging fluorescence microscopy: spatial heterogeneity of photobleaching rate constants in individual cells. *J. Cell. Biol.* 100:1309–1323.

Burg, M., J. Grantham, M. Abramow, and J. Orloff. 1966. Preparation and study of fragments of single rabbit nephrons. *Am. J. Physiol.* 210:1293–1298.

Chary, S. R., and R. K. Jain. 1989. Direct measurement of interstitial convection and diffusion of albumin in normal and neoplastic tissues by fluorescence photobleaching. *Proc. Natl. Acad. Sci. USA.* 86:5385–5389.

Chen. P.-Y., D. Pearce, and A. S. Verkman. 1988. Membrane water and solute permeability determined quantitatively by self-quenching of an entrapped fluorophore. *Biochemistry.* 27:5713–5718.

Crank, J. 1956. The Mathematics of Diffusion. Clarendon Press, Oxford.

Edidin, M., Y. Zagyansky, and T. J. Lardner. 1976. Measurement of membrane protein lateral diffusion in single cells. *Science (Wash. DC).* 191:466–468.

Ellis, G. W. 1979. A fiber-optic phase-randomizer for microscope illumination by laser. *J. Cell Biol.* 83:303*a*. (Abstr.)

Flamion, B., and K. R. Spring. 1990. Water permeability of apical and basolateral cell membranes of rat inner medullary collecting duct. *Am. J. Physiol.* 259:F986–F999.

Icenogle, R. D. 1981. Fluorescence correlation spectroscopy and fluorescence photobleaching recovery studies of the binding of ethidium to deoxyribonucleic acid. Ph.D. thesis. Cornell University, Ithaca, NY.

Jacobson, K., E. Wu, and G. Poste. 1976. Measurement of the translational mobility of concanavalin A in glycerol-saline solutions and on the cell surface by fluorescence recovery after photobleaching. *Biochim. Biophys. Acta.* 433:215–222.

Kapitza, H.-G., and E. Sackmann. 1980. Local measurement of lateral motion in erythrocyte membranes by photobleaching technique. *Biochim. Biophys. Acta.* 595:56–64.

Kaufman, E. N., and R. K. Jain. 1990. Quantification of transport and binding parameters using fluorescence recovery after photobleaching. Potential for in vivo applications. *Biophys. J.* 58:873–885.

Kuwahara, M., C. A. Berry, and A. S. Verkman. 1988. Rapid development of vasopressin-induced hydrosmosis in kidney collecting tubules measured by a new fluorescence technique. *Biophys. J.* 54:595–602.

Lanni, F., D. L. Taylor, and B. R. Ware. 1981. Fluorescence photobleaching recovery in solutions of labeled actin. *Biophys. J.* 35:351–364.

Lew, H. S., and Y. C. Fung. 1969. On the low-Reynolds-number entry flow into a circular cylindrical tube. *J. Biomech.* 2:105–119.

Peters, R. 1984. Nucleo-cytoplasmic flux and intracellular mobility in single hepatocytes measured by fluorescence microphotolysis. *EMBO (Eur. Mol. Biol. Organ.) J.* 3:1831–1836.

Peters, R., J. Peters, K. H. Tews, and W. Bahr. 1974. A microfluorimetric study of translational diffusion in erythrocyte membranes. *Biochim. Biophys. Acta.* 367:282–294.

Petersen, N. O., S. Fedler, and E. L. Elson. 1986. Measurement of lateral diffusion by fluorescence photobleaching recovery. *In* Handbook of Experimental Immunology. D. M. Weir, L. A. Herzenberg, C. Blackwell, and Leonore A. Blackwell, editors. Blackwell Scientific Publications, Oxford, UK. 24.1–24.23.

Salmon, E. D., R. J. Leslie, W. M. Saxton, M. L. Karow, and J. R. McIntosh. 1984. Spindle microtubule dynamics in sea urchin embryos: analysis using a fluorescein-labeled tubulin and measurements of fluorescence redistribution after laser photobleaching. *J. Cell Biol.* 99:2165–2174.

Simon, J. R., A. Gough, E. Urbanik, F. Wang, F. Lanni, B. R. Ware, and D. L. Taylor. 1988. Analysis of rhodamine and fluorescein-labeled F-actin diffusion in vitro by fluorescence photobleaching recovery. *Biophys. J.* 54:801–815.

Spring, K. R. 1990. Quantitative imaging at low light levels: differential interference contrast and fluorescence microscopy without significant light loss. *In* Optical Microscopy for Biology. B. Herman, and K. A. Jacobson, editors. Wiley-Liss, New York. 513–522.

Spring, K. R., and P. D. Smith. 1987. Illumination and detection systems for quantitative fluorescence microscopy. *J. Micros.* 147:265–278.

Strange, K., and K. R. Spring. 1986. Methods for imaging renal tubule cells. *Kidney Int.* 30:192–200.

Verkman, A. S. Mechanisms and regulation of water permeability in renal epithelia. 1989. *Am. J. Physiol.* 257:C837–C850.

Wade, M. H., J. E. Trosko, and M. Schindler. 1986. A fluorescence photobleaching assay of gap junction-mediated communication between human cells. *Science (Wash. DC).* 232:525–528.

Wells, K. S., D. R. Sandison, J. Strickler, and W. W. Webb. 1989. Quantitative fluorescence imaging with laser scanning confocal microscopy. *In* The Handbook of Biological Confocal Microscopy. J. Pawley, editor. IMR Press, University of Wisconsin, Madison, WI. 23–35.

Wojcieszyn, J. W., R. A. Schlegel, E.-S. Wu, and K. A. Jacobson. 1981. Diffusion of injected macromolecules within the cytoplasm of living cells. *Proc. Natl. Acad. Sci. USA.* 78:4407–4410.

Wolf, D. E. 1989. Designing, building, and using a fluorescence recovery after photobleaching instrument. *In* Methods in Cell Biology. Y.-L. Wang, and D. L. Taylor, editors. Academic Press, New York. 271–306.